JOURNAL OF SOLID STATE CHEMISTRY **133,** 466–472 (1997)
ARTICLE NO. SC977511

Electrical Transport in Semiconducting $(LaMn_{1-x}Ti_x)_{1-y}O_3$ ($x \leq 0.05$)

W. H. Jung,[1] H. Nakatsugawa, and E. Iguchi

Materials Science, Department of Mechanical Engineering and Materials Science, Faculty of Engineering, Yokohama National University, Tokiwadai, Hodogaya-Ku, Yokohama 240, Japan

Received December 23, 1996; in revised form April 29, 1997; accepted June 12, 1997

Electrical transport properties in the ceramic specimens of $(LaMn_{1-x}Ti_x)_{1-y}O_3$ system ($x \leq 0.05$) have been investigated as a function of temperature by the complex-plane impedance analyses, dielectric properties, four-probe DC conductivities, and Seebeck coefficients. The complex-plane impedance analysis distinguishes the bulk conduction from the conduction across the grain boundaries. The bulk conduction contains two thermally activated processes separated at the Néel temperature (T_N). A dielectric relaxation appears in a loss tangent and electric modulus below T_N. The activation energy required for the relaxation is nearly equal to that for the conduction at $T < T_N$. The electrical transport below T_N is explained self-consistently in terms of a hopping process of small polarons of holes, which are formed by a superexchange interaction and are more deeply localized by the assistance of the Jahn–Teller effect. A correlation between the bulk conduction at $T > T_N$ and the hopping process of small polarons of holes is also discussed.

INTRODUCTION

The manganese-based perovskite, $La_{1-x}D_xMnO_3$ (D a divalent alkaline earth such as Ca, Sr, or Ba), forms a Mn^{3+}/Mn^{4+} mixed-valence system for $x > 0$, which exhibits interesting and coupled magnetic transport properties (1–6). The transport properties in $La_{1-x}D_xMnO_3$ systems have been traditionally examined within the framework of a double exchange interaction due to the magnetic coupling between Mn^{3+} and Mn^{4+} (7–12).

Using a simplified double exchange Hamiltonian, however, the recent calculation of the magnetic field-dependent resistivity of hole-doped $LaMnO_3$ near the metal–insulator (MI) transition by Mills *et al.* shows inconsistency with the experimental results (13), and alternatively they have proposed that a Jahn–Teller-type electron–phonon coupling plays an important role in the electrical transport in this material, that is, a polaron picture would be a better model for the transport properties. Millis (14) has also calculated the energy gained by the formation of the local lattice distortion due to the Jahn–Teller effect using a classical model. He also suggests a strong electron–phonon coupling, and his calculation supports the polaronic transport in hole-doped $LaMnO_3$. In fact, many entries in the current literature (15–18) reported that the majority carriers responsible for the conduction in nonmetallic phases of hole-doped $LaMnO_3$ were small polarons which were widely believed to be stabilized by the assistance of the Jahn–Teller-type electron–phonon interaction. The dynamics of small polarons is indispensable in the interpretation of electrical transport properties in Mn-based perovskite materials, but the effects of small polarons have not been taken into consideration enough in the transport properties.

Although the recent attention has been focused predominantly on hole-doped $LaMnO_3$, there have been no reports on the conduction properties in the electron-doped $LaMnO_3$ which is created by the substitution of tetravalent ions for Mn. In the present work, therefore, we have investigated transport properties in the perovskite-type system of $LaMn_{1-x}Ti_xO_3$ ($x \leq 0.05$), which must provide very important information on both the nature of charge carriers and the characteristic electrical conduction in manganese oxides. The substitution of Ti for Mn would induce several effects. One of the most significant effects is a decrease in hole (Mn^{4+}) density because a Ti^{4+} ion generates an electron, which is subject to the electrical neutrality.

In the various experimental means which can address the polaron dynamics, dielectric properties provide important knowledge because a hopping process of small polarons has a high possibility to involve a dielectric relaxation. In fact, our previous reports (19–25) show that a dielectric relaxation presents significant experimental results leading directly to electrical characterization, particularly of localized carriers such as polarons and also to a transport kinetics due to hopping carriers. In order to correlate the charge dynamics (and/or polaron dynamics) with the electrical transport mechanism, a high-quality crystal is required. This is mainly because the ceramics samples suffer from the carrier scattering in grain boundaries. Therefore, the use of

[1] To whom correspondence should be addressed.

0022-4596/97 $25.00

single crystals surely relieves most problems. Growth of a single crystal is generally very difficult in comparison with the conventional preparation of oxides by sintering. Even if a polycrystalline ceramic specimen is employed, however, the complex-plane impedance analysis distinguishes the bulk conduction from the conduction across the grain boundary and the transport across the electrode–specimen interface, if they exist (26, 27). The combination of the complex-plane impedance analysis and the dielectric measurement could be then one of the strongest means for the investigation of electrical transports in polycrystalline $LaMn_{1-x}Ti_xO_3$.

To this end, the present study measures DC conductivities, dielectric properties, and Seebeck coefficients in $LaMn_{1-x}Ti_xO_3$ as a function of temperature and discusses the possibility of the electrical transport due to a hopping process of small polarons of holes, considering the local lattice distortion due to the Jahn–Teller-type electron–phonon coupling.

EXPERIMENTAL

Polycrystalline samples of $LaMn_{1-x}Ti_xO_3$ ($x = 0.00$, 0.03, and 0.05) were prepared by solid-state reaction. The starting materials were La_2O_3, $MnCO_3$, and TiO_2 (Johnson Matthey, 5N Grade). La_2O_3 was first fired in air at 1273 K for 12 h. $MnCO_3$ was also calcined in air at 1473 K for 24 h to form Mn_3O_4. These powders were mixed and then calcined in air at 1373 K for 24 h. After being ground again, mixed well, and pressed into pellets, they were finally fired on platinum foil at 1623 K for 48 h in air. To characterize the crystal, X-ray diffraction measurements, as well as energy dispersive X-ray spectroscopy (EDX), were carried out. It has been well known that $LaMnO_3$ exhibits oxygen excess nonstoichiometry (28). The Mn^{4+} content was determined by redox titration using the standard ferrous and permanganate solutions. Then Mn^{4+} contents in the present materials are 14, 9, and 5% for $x = 0.00$, 0.03, and 0.05, respectively. In this case, the chemical formula was generally given as $LaMn_{1-x}Ti_xO_{3+\delta}$, but it is better written as $(LaMn_{1-x}Ti_x)_{1-\gamma}O_3$, reflecting the presence of cation vacancies rather than excess oxygen (28). Thus, the chemical formulae for our specimens would be represented as $(LaMn)_{0.977}O_3$, $(LaMn_{0.97}Ti_{0.03})_{0.98}O_3$, and $(LaMn_{0.95}Ti_{0.05})_{0.984}O_3$ for $x = 0.00$, 0.03, and 0.05, respectively. EDX data confirmed the presence of cation vacancies in the crystals.

X-ray photoelectron spectra (XPS) were measured at room temperature with a commercial X-ray photoelectron spectrometer (PHI ESCA-5600). The base pressure in the chamber was about 10^{-12} atm. The X-ray source is the monochromatized Al$K\alpha$ line (1486.6 eV) with a combined energy resolution of about 0.3 eV. The cleanliness of a sample surface was ensured by *in situ* scraping of the surface with an alumina file, so that the C 1*s* signal due to carbonate impurity in the surface was found to be very weak in all of the samples. Core level binding energies were assigned with respect to the C 1*s* peak at 284.6 eV as a reference in order to account for the surface charge up. The Mn $2p_{3/2}$ core level binding energy for $x = 0.05$, for instance, appears at about 641.1 eV which moves slightly to a higher energy level as x decreases. According to XPS experiment result for $LaMnO_{3+\delta}$ carried out by Chainani *et al.* (29), indeed, the Mn $2p_{3/2}$ core level binding energy is observed at 642.1 eV. Our XPS results, therefore, imply that the increase in x results in a decrease in concentration of Mn^{4+}.

We have also carried out XPS experiment to examine the valency of Ti ions. The Ti 2*p* core level binding energy in the present materials is observed to be at about 457.3 eV. In general, the valency of Ti ions in $(LaMn_{1-x}Ti_x)_{1-\gamma}O_3$ is very difficult to determine because the crystal field parameter of Ti^{4+}, $10Dq$, is very close in values to that of Ti^{3+} (30, 31). In the XPS spectra by Fujimori *et al.* (30), the Ti 2*p* core level spectrum for Ti^{3+} in $LaTiO_3$ which involves 15% Ti^{4+} includes a sharp peak at 457 eV and a shoulder at 462.5 eV (30), while the Ti 2*p* core level binding energy for Ti^{4+} in $SrTiO_3$ is observed at 458.8 eV (31). Although there is a possibility that some Ti^{4+} ions in $(LaMn_{1-x}Ti_x)_{1-\gamma}O_3$ transfer to Ti^{3+} because of oxygen deficiency due to ultra-high vacuum, the valency of Ti ions in our samples would be nearly 4+ on average, as expected. If the valency of Ti ion in $(LaMn_{1-x}Ti_x)_{1-\gamma}O_3$ is 3+, Ti^{3+} ion should generate Mn^{2+} and then the Mn $2p_{3/2}$ core level must shift toward a lower level because a binding energy of a core level shifts generally toward the lower side when the valency is reduced (29).

Powder X-ray diffraction patterns correspond well to the pattern reported by Verelst *et al.* (32). $(LaMn_{1-x}Ti_x)_{1-\gamma}O_3$ has the $GdFeO_3$-type orthorhombic perovskite structure. In our experiment, we tried to increase x up to 0.1 but found that $x = 0.07$ was the upper limit to obtain a single phase sample by the conventional solid-state reaction technique in air. The densities of the specimens were about 90% of the theoretical values, which were calculated using the lattice constants obtained in X-ray measurements.

A Keithley 619 Resistance Bridge, an Advantest TR 6871 digital multimeter, and an Advantest R 6161 power supply were used for DC conductivity measurements by the four-probe method. Seebeck coefficients were measured with a precision digital multimeter in the temperature range of about 100 to 300 K in a home-made device. Using HP 4274A, 4275A, and 4284A LCR meters with the frequency range of 100 Hz to 1 MHz, capacitances and conductances were obtained as a function of temperature up to 300 K by four-terminal pair AC impedance measurements. The measured values of capacitances and conductances were corrected by calibrating capacitances and resistances of leads to zero. An In–Ga alloy in 7 : 3 ratio was used for the electrode of measurements of capacitances and conductances.

In order to check Maxwell–Wagner-type polarization, capacitance measurements were carried out at 80 K in the frequency range of 1 kHz–1 MHz by changing the thickness of the specimen from 1.2 to 0.6 mm. The dielectric constants were then found to be independent of the thickness of the specimen. Consequently, Maxwell–Wagner-type polarization is excluded. To test the effect of the electrode–specimen interface, evaporated gold was also used, but there were no differences in the experimental results. The theoretical framework of the complex impedance analysis employed in this work (26, 27) and the further detailed experimental procedures are well described elsewhere (19–25).

RESULTS

Figure 1 shows the temperature dependence of the Seebeck coefficients (α) for every specimen. Positive Seebeck coefficients indicate that the $(LaMn_{1-x}Ti_x)_{1-\gamma}O_3$ system is a *p*-type semiconductor in the temperature range where the coefficients can be measured. The resistances of our samples were greater than about $10^6\ \Omega$ below 100 K. Such a high resistance makes the open-circuit-like noise greater than the signal. With increasing x, α increases. The maxima of the coefficients appear around 160 K, near the Néel temperature (T_N) in $LaMnO_3$. $LaMnO_3$ is an antiferromagnetic insulator below $T_N = 140$ K (33).

Figure 2 depicts complex-plane impedance plots at 92, 130, and 200 K for $x = 0.00$. The plots at 92 and 130 K contain two semicircular arc structures, i.e., the highest-frequency arc crossing through the origin (the bulk conduction) and the intermediate arc (the conduction across the grain boundary). Though the highest-frequency arc appears below 140 K, the plots of this arc at higher temperatures require frequencies much higher than the maximum one in the present study (see Fig. 2c). The lowest resistance value of the intermediate arc corresponds to the bulk resistance. Since the lowest-frequency arc was not observed in every specimen, there must be no electrode polarization in the present system throughout the frequencies employed in the measurements. The highest resistance value of the intermediate arc is the total resistance in the grains and grain boundaries (26, 27).

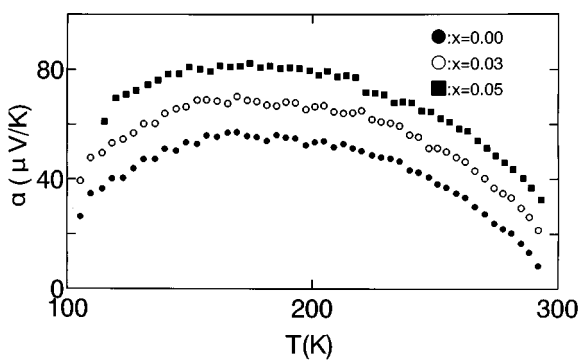

FIG. 1. Temperature dependencies of Seebeck coefficients, α, as a parametric function of the amount of Ti, i.e., x.

The Arrhenius relations plotting the bulk conductivities and those corresponding to the highest resistance values of the intermediate arcs against reciprocal temperatures are illustrated in Fig. 3 together with DC conductivities for the specimen of $x = 0.03$. Since most of the conductivities corresponding to the highest resistance values of the intermediate arcs overlap the DC conductivities, the four-probe method measures the total resistances in the grains and boundaries. The bulk conductivities estimated from the lowest resistance values of the intermediate arcs above 140 K are extrapolated on the line from the low temperature region. This fact suggests that a dielectric relaxation occurs within the grains even above 140 K, as expected.

Employing the bulk conductivities, Fig. 4 plots Arrhenius relations of σT and $1/T$. In every specimen, there is a transition from the low-temperature conduction process to the high-temperature one, i.e., the linear portion at $T <$ 140 K with an activation energy of 0.085, 0.092, or 0.12 eV and another one at $T > 200$ K with an activation energy of 0.16, 0.17, or 0.19 eV for the specimen of $x = 0.00$, 0.03, or 0.05. It is noteworthy that the conductivities decrease with an increase in x. Furthermore, the activation energies required for both the conduction processes increase as x increases.

Figure 5 displays the frequency dependencies of the dielectric loss tangent and electric modulus for the specimen of $x = 0.05$ at several temperatures. Above 120 K, no resonance peak was recognized in the frequency range employed in the present work. This fact implies that the resonance peak disappears at high temperatures or the dielectric relaxation process requires the frequencies much higher than 1 MHz, the maximum frequency used in the present work, if it exists above 120 K.

DISCUSSION

The present study has succeeded in distinguishing the bulk conduction from the conduction across grain boundaries, using the complex-plane impedance analyses. The bulk conductivities obtained by the impedance analyses are remarkably higher than those by the four-probe DC technique as shown in Fig. 3. The elucidation of the real transport behaviour requires the bulk conduction.

The temperature dependencies of the conductivities in Fig. 4 resemble closely those of $LaFe_xNi_{1-x}O_3$ ($x \leq 0.2$), $LaCoO_3$, and $Nd_{1-x}La_xNiO_3$ ($x \leq 0.3$) which include rather deeply localized 3*d* electrons (34–36). In these systems, the electrical transport properties have been explained in terms of the polaron hopping conduction. If the conduction is due to a hopping-process of small polarons of holes,

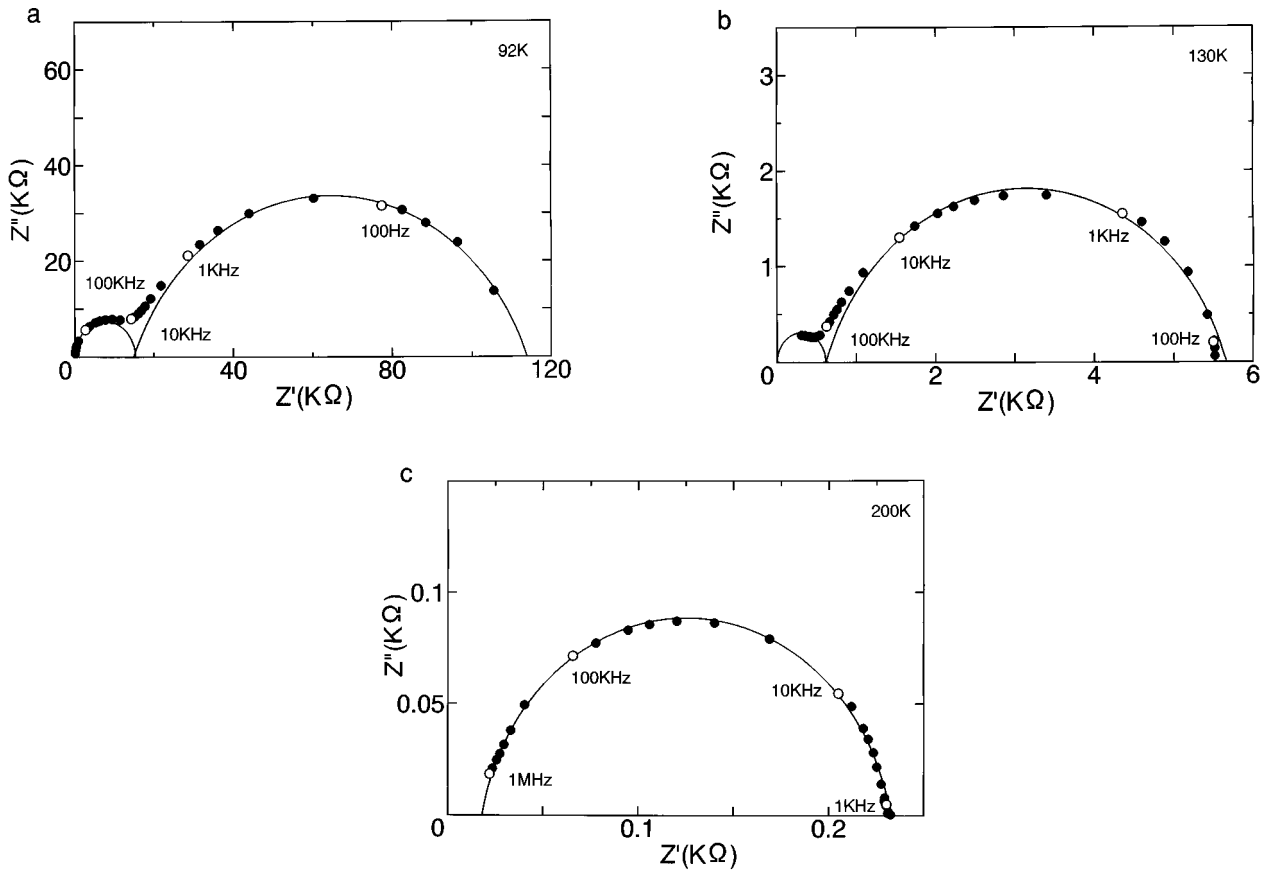

FIG. 2. The complex-plane impedance analyses for the specimen of $x = 0.00$ at several temperatures: (a) 92 K, (b) 130 K, and (c) 200 K, where Z' and Z'' represent the real and imaginary parts of the total impedance at each applied frequency, respectively.

the temperature dependence of the bulk conductivity predicted by polaron theory is of the form (19–25, 34, 35, 37, 38)

$$\sigma T \propto \exp\left(-\frac{W_H + W_D/2}{k_B T}\right), \qquad [1]$$

where W_H is the hopping energy of a polaron and W_D represents the disordered energy which is generally negligibly small in a crystalline bulk, even less than the experimental error in the determination of W_H (39). The linear relations in the Arrhenius plots of σT and $1/T$ in Fig. 4 are surely in favor of the polaronic conduction in $(LaMn_{1-x}Ti_x)_{1-\gamma}O_3$ system. As shown in Fig. 4, however, this system contains two bulk conduction processes, one above T_N and another below T_N.

The discussion starts from the low-temperature conduction process in the antiferromagnetic phase below T_N. As demonstrated in Fig. 5, the dielectric relaxation process takes place below T_N. Dielectric relaxation behavior is approximately described by Debye's theory (35, 38). The dielectric loss tangent and dielectric modulus are

$$\tan\delta = \frac{\varepsilon''}{\varepsilon'} = (\varepsilon_0 - \varepsilon_\infty)\frac{\omega\tau_0}{\varepsilon_0 + \varepsilon_\infty(\omega\tau_0)^2}, \qquad [2]$$

$$M'' = (\varepsilon_0 - \varepsilon_\infty)\frac{\omega\tau_0}{\varepsilon_0^2 + \varepsilon_\infty^2(\omega\tau_0)^2}, \qquad [3]$$

where $M^* = M' + jM'' = 1/(\varepsilon' - \varepsilon'')$ and $\tau_0 = (\varepsilon_0 + 2)\tau/(\varepsilon_\infty + 2)$. At a temperature T, the loss tangent ($\tan\delta$) and the electric modulus (M'') have the maxima at the resonance frequencies, $f_{\tan\delta}$ and f_M, i.e., $f_{\tan\delta} = \sqrt{\varepsilon_0/\varepsilon_\infty}/2\pi\tau$ and $f_M = (\varepsilon_0/\varepsilon_\infty)/2\pi\tau$, where ε_0 and ε_∞ are the static and high-frequency dielectric constants, and τ is the relaxation time, which is proportional to $\exp(Q/k_B T)$, Q being the activation energy for the dielectric relaxation. These relations yield the dielectric resonance condition at a temperature T (35, 40) as

$$\frac{(f_{\tan\delta})^2}{f_M} \propto \exp\left(-\frac{Q}{k_B T}\right). \qquad [4]$$

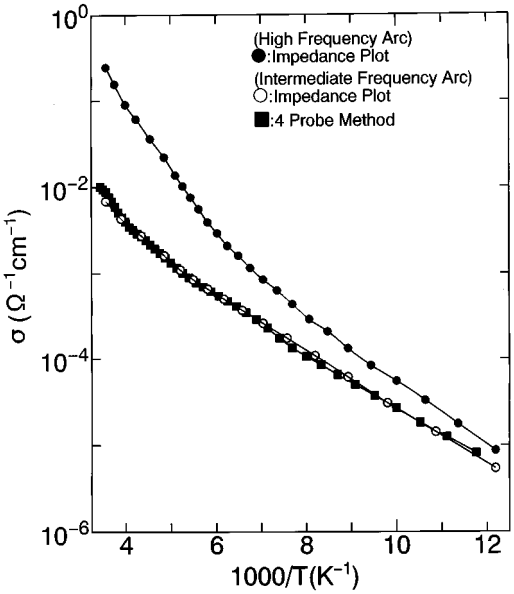

FIG. 3. Three Arrhenius relations of σ vs $1/T$ for the specimen of $x = 0.03$ below room temperature; the first one (solid circles) represents the bulk conductivities obtained from the real axis intercepts of the highest frequency arcs in the impedance analyses, the second one (open circles) employs the highest resistance values of the intermediate semicirculars, and the third one (solid squares) is plotted using the DC conductivities measured by the four-probe method.

Figure 6 plots the Arrhenius relations of $(f_{\tan\delta})^2/f_M$ and $1/T$. Good straight lines are obtained with $Q = 0.08$, 0.09, and 0.12 eV for the specimens of $x = 0.00$, 0.03, and 0.05, respectively. These values are in good agreement with the

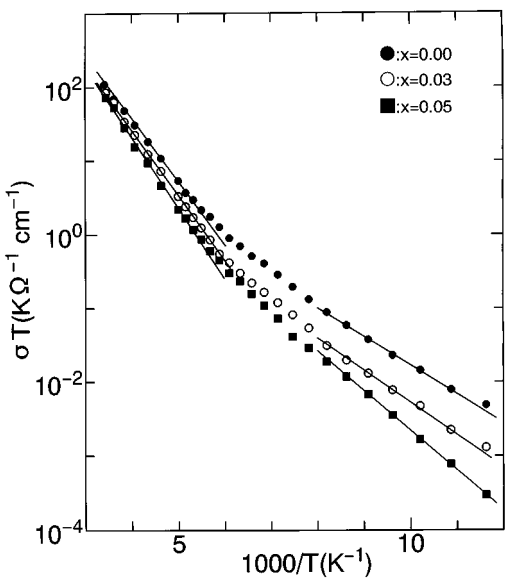

FIG. 4. Arrhenius relations between σT and $1/T$, where σ is the bulk conductivity. Each specimen contains two thermally activated processes represented by the straight solid lines.

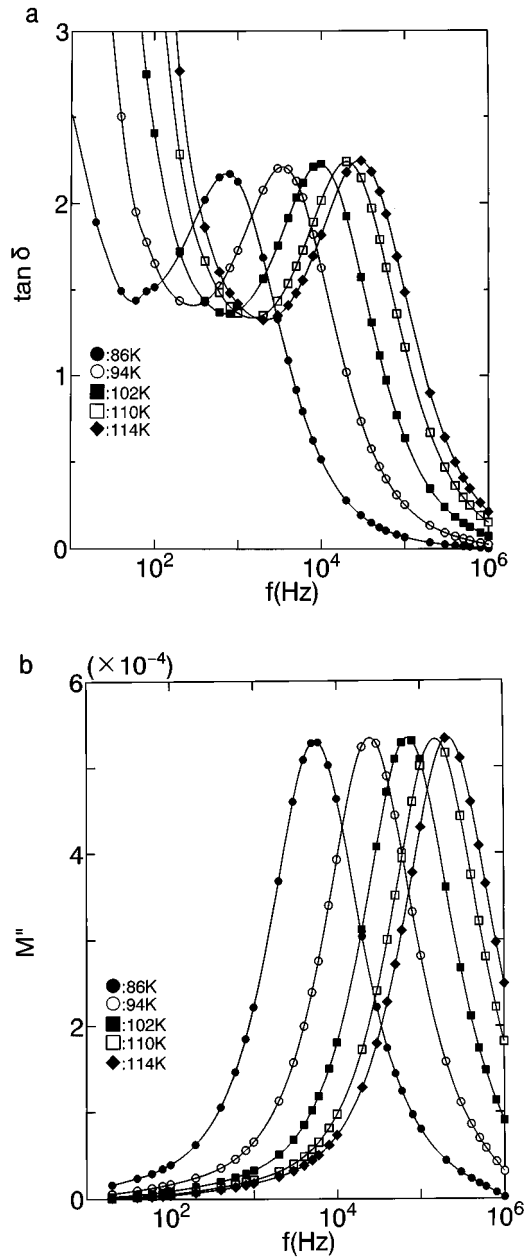

FIG. 5. Frequency dependencies of dielectric loss tangent ($\tan\delta$) and electric modulus (M'') at several temperatures for the specimen of $x = 0.05$; (a) $\tan\delta$ and (b) M''.

activation energies required for the bulk conduction, which are obtained in Fig. 4, i.e., $Q \cong W_H$. If the bulk conduction process does not contain a dielectric relaxation, the impedance analysis theory indicates that the imaginary parts in the highest-frequency semicircle become zero, as Maiti and Basu (41) demonstrated on electron-doped $BaTiO_3$. If $\theta = \pi$ in the highest-frequency arc, on the other hand, only the conduction process associated with a dielectric relaxation leads to the bulk conduction and consequently the

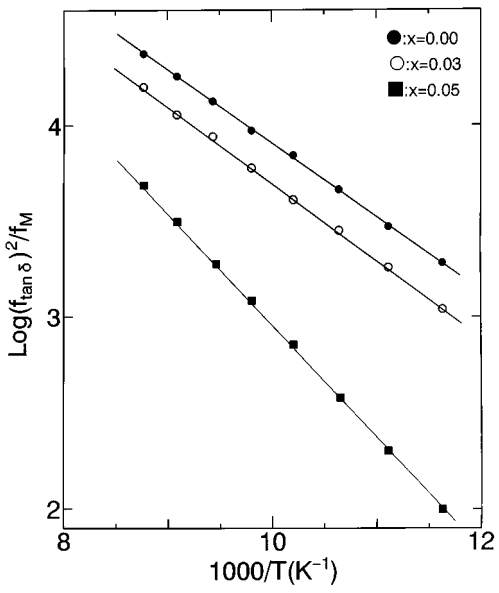

FIG. 6. Arrhenius relations between $(f_{\tan\delta})^2/f_M$ and $1/T$.

activation energy required for the bulk conduction is equal to that for the dielectric relaxation, i.e., $Q = W_H$, where θ is the angle of the origin—the center of the highest-frequency arc—the real axis intercept (41). Besides the hopping energy of small polarons, the bulk conduction due to a hopping process of small polarons generally involves the energy required for creation of free small polarons (e.g., see (35)). In this case, $W_H > Q$ as shown in our previous reports (19–25, 34, 35). In $(LaMn_{1-x}Ti_x)_{1-\gamma}O_3$ system, θ is nearly equal to π (i.e., $\theta \cong 0.96\pi$) and then $Q \cong W_H$. This fact implies that the hopping process of small polarons of holes dominates the electrical transports below T_N (35).

According to the recent studies on photoemission and XAS by Saitoh *et al.* (42), $LaMnO_3$ is a charge transfer (CT)-type insulator with the ground state of strongly p–d mixed character because of strongly hybridization of Mn 3d and O 2p. Taking into account their optical results, the XPS results on our samples, and the fact that the hopping process of small polarons of holes takes place, therefore, the hopping of mobile charge carriers between O 2p and Mn 3d orbitals would be preponderant over the hopping between singly occupied e orbitals on Mn^{3+} ions ($t_{2g}^3 e_g^1$) and empty e orbitals of $Mn^{4+}(t_{2g}^3)$ (43, 44). In fact, the similar hopping processes occur with the assistance of the antiferromagnetic ordering due to superexchange interactions in several related 3d transition metal compounds (45, 46). Furthermore, the temperature dependencies of Seebeck coefficients observed in Fig. 1 are similar to those in the systems with strong hybridization of O 2p and 3d orbitals (47–49).

From this point of view, the charge carriers attributing to the electrical conduction below T_N are small polarons of holes. Since Mn^{3+} ions in a high-spin state introduce generally a tetragonal distortion due to a Jahn–Teller effect (42–44), these small polarons of holes must be more deeply localized and/or more surely stabilized by the assist of the Jahn–Teller effect (13, 14). According to the small polaron theory, a decrease in the concentration of small polarons results in an increase in the hopping energy (38), and then the stability and/or localization of small polarons is closely related to the polaron binding energy (W_P) because the increase in the polaron binding energy enhances the stability and/or localization of small polarons. Furthermore, the Jahn–Teller-type electron–phonon interaction may enlarge the polaron binding energy because the potential energy of an electron (and/or a hole) is lowered by the displacement of the neighboring ions introduced by the electron–phonon interactions. Thus, a strong electron–phonon interaction induces large displacement of ions, which localizes electrons (and/or holes) more deeply and consequently results in a large value for the polaron binding energy (50). As x in $(LaMn_{1-x}Ti_x)_{1-\gamma}O_3$ increases, the activation energy required for the bulk conduction increases (see Fig. 4) as do the Seebeck coefficients (see Fig. 1). These increases provide the direct support for the theoretical picture described above because $W_P \cong 2W_H$ (38). Consequently, the hopping energies required for the bulk conduction increase with increasing x, and the superexchange interaction and the Jahn–Teller effect must cooperate in the electrical transports due to the hopping process of small polarons of holes in the antiferromagnetic phase below T_N.

The temperature dependencies of conductivities above T_N also suggest polaronic conduction, but the energies required for the conduction are higher than those below T_N. The Jahn–Teller effect may still contribute to the hopping process of small polarons of holes in the paramagnetic phase, because this effect works even above T_N. However, the superexchange interaction should become less prominent or disappear in a paramagnetic phase (44, 51). It is generally accepted that charge carriers in a paramagnetic phase are localized more deeply by a spin disorder (16), therefore the nature of the small polarons of holes changes from that below T_N, and this must be one of the main reasons which result in the high hopping energies above T_N.

Though the Arrhenius relation of σT and $1/T$ above T_N in Fig. 4 favors small polaron hopping conduction, some more direct evidence by other experimental means is required. Dielectric measurements especially, using frequencies much higher than those in the present work, could provide direct evidence if a hopping process of small polarons of holes dominates the bulk conduction at $T > T_N$, as Mills *et al.* suggested (13, 14).

CONCLUSION

The present paper has succeeded in distinguishing the bulk conduction from the conduction across grain boundaries

in the $(LaMn_{1-x}Ti_x)_{1-y}O_3$ system ($x = 0.0$, 0.03, and 0.05). In the temperature dependencies of the bulk conductivities, there are two thermally activated processes separated at the Néel temperature, T_N. Below T_N, a dielectric relaxation appears in every specimen and the activation energy required for the relaxation is nearly equal to the activation energy in the bulk conduction. Above T_N, a dielectric relaxation process requires frequencies higher than the maximum one in the present study. In the antiferromagnetic phase below T_N, the electrical transport in the bulk proceeds via a hopping process of small polarons of holes between O $2p$ and Mn $3d$ orbitals. Both a superexchange interaction and the Jahn–Teller effect contribute to the hopping process of small polarons of holes. The x dependencies of the conductivities and Seebeck coefficients indicate that small polarons of holes are the most plausible candidates for the majority carriers, where x represents the amount of Ti ions. In the paramagnetic phase above T_N, the temperature dependencies of the bulk conductivities also suggest a possibility of the polaronic conduction with activation energies higher than those below T_N, but more direct evidence by other experimental means is required to confirm this possibility.

ACKNOWLEDGMENTS

The authors are very grateful to F. Munakata, K. Ueda, and K. Okamoto for the useful advice, the assistance in this project, and useful discussion. This project was supported by a Grant-in-Aid for Science Research (No. 08650812) from the Ministry of Education, Science and Culture, Japan.

REFERENCES

1. R. von Helmont, J. Wecker, B. Holzapfel, L. Schultz, and K. Samwer, *Phys. Rev. Lett.* **71,** 2331 (1993).
2. M. McCormack, S. Jin, T. H. Tiefel, R. M. Fleming, J. M. Phillips, and R. Ramesh, *Appl. Phys. Lett.* **64,** 3045 (1994).
3. Y. Tokura, A. Urushibara, Y. Moritomo, T. Arima, A. Asamitsu, G. Kido, and N. Furukawa, *J. Phys. Soc. Jpn.* **63,** 3931 (1994).
4. S. Jin, T. H. Tiefel, M. McCormack, R. A. Fastnacht, R. Ramesh, and L. H. Chen, *Science* **264,** 413 (1994).
5. H. L. Ju, C. Kwon, Li Qi, R. H. Greene, and T. Venkatesan, *Appl. Phys. Lett.* **65,** 2108 (1994).
6. A. Asamitsu, Y. Tomioka, Y. Moritomo, T. Arima, and Y. Tokura, *Nature* **373,** 407 (1995).
7. G. H. Jonker and J. H. van Santen, *Physica* **16,** 337 (1950).
8. G. H. Jonker and J. H. van Santen, *Physica* **19,** 120 (1953).
9. C. Zener, *Phys. Rev.* **82,** 403 (1951).
10. P. W. Anderson and H. Hasegawa, *Phys. Rev.* **100,** 675 (1955).
11. P. G. de Gennes, *Phys. Rev.* **118,** 141 (1960).
12. Y. Okimoto, T. Katsufuji, T. Ishikawa, A. Urushibara, T. Arima, and Y. Tokura, *Phys. Rev. Lett.* **75,** 109 (1995).
13. A. J. Mills, P. B. Littlewood, and B. I. Shraiman, *Phys. Rev. Lett.* **74,** 5144 (1995).
14. A. J. Millis, *Phys. Rev. B* **53,** 8434 (1996).
15. T. A. Tyson, J. Mustre de Leon, S. D. Conradson, A. R. Bishop, J. J. Neumeier, H. Röder, and Jun Zang, *Phys. Rev. B* **53,** 13985 (1996).
16. V. H. Crespi, L. Lu, Y. X. Jia, K. Khazeni, A. Zettle, and M. L. Cohen, *Phys. Rev. B* **53,** 14303 (1996).
17. W. Archibald, J. S. Zhou, and J. B. Goodenough, *Phys. Rev. B* **53,** 14445 (1996).
18. M. Jaime, M. B. Salamon, M. Rubinstein, R. E. Treece, J. S. Horwitz, and D. B. Chrisey, *Phys. Rev. B* **54,** 11914 (1996).
19. E. Iguchi, N. Kubota, T. Nakamori, N. Yamamoto, and K. J. Lee, *Phys. Rev. B* **43,** 8646 (1991).
20. E. Iguchi and K. Akashi, *J. Phys. Soc. Jpn.* **61,** 3385 (1992).
21. K. J. Lee, A. Iguchi, and E. Iguchi. *J. Phys. Chem. Solids* **54,** 975 (1993).
22. E. Iguchi and W. H. Jung, *J. Phys. Soc. Jpn.* **63,** 3078 (1994).
23. W. H. Jung and E. Iguchi, *J. Phys.: Condens. Matter.* **7,** 1215 (1995).
24. E. Iguchi, T. Hasimoto, and S. Yokoyama, *J. Phys. Soc. Jpn.* **65,** 221 (1996).
25. E. Iguchi and N. Nakamura, *J. Phys. Chem. Solids* **58,** 755 (1997)
26. J. R. MacDonald, *J. Chem. Phys.* **61,** 3977 (1974).
27. A. O. Franklin, *J. Am. Ceram. Soc.* **58,** 465 (1975).
28. J. A. M. van Roosmalen, E. H. P. Cordfunke, R. B. Helmholdt, and H. W. Zandbergen, *J. Solid State Chem.* **110,** 100 (1994).
29. A. Chainani, M. Mathew, and D. D. Sarama, *Phys. Rev. B* **47,** 15379 (1993).
30. A. Fujimori, I. Hase, M. Nakamura, H. Nakatame, Y. Fujishima, Y. Tokura, M. Abbate, F. M. de Groot, M. T. Czyzyk, J. C. Fuggle, O. Strebel, F. Kopez, M. Domke, and G. Kaindle, *Phys. Rev. B* **46,** 9841 (1992).
31. M. Murata, K. Wakino, and S. Ikeda, *J. Electron Spectrosc. Relat. Phenom.* **6,** 459 (1975).
32. M. Verelst, N. Rangavittal, C. N. R. Rao, and A. Rousset, *J. Solid State Chem.* **104,** 74 (1993).
33. E. O. Wollan and W. C. Koehler, *Phys. Rev.* **100,** 545 (1955).
34. W. H. Jung and E. Iguchi, *Philos. Mag. B* **73,** 873 (1996).
35. E. Iguchi, K. Ueda, and W. H. Jung, *Phys. Rev. B* **54,** 17431 (1996).
36. L. Blasco and J. García, *J. Phys.: Condens. Matter* **6,** 10759 (1994).
37. D. Emin and T. Holstein, *Ann. Phys.* **53,** 439 (1969).
38. I. G. Austin and N. F. Mott, *Adv. Phys.* **18,** 41 (1969).
39. L. A. K. Dominik and MacCrone, *Phys. Rev.* **163,** 757 (1967).
40. R. Gerhardt, *J. Phys. Chem. Solids* **55,** 1491 (1994).
41. H. S. Maiti and R. N. Basu, *Mater. Res. Bull.* **21,** 1107 (1986).
42. T. Saitoh, A. E. Bocquet, T. Mizokawa, H. Namatame, A. Fujimori, M. Abbate, Y. Takeda, and M. Takano, *Phys. Rev. B* **51,** 13942 (1995).
43. S. Satpathy, Z. S. Popović, and F. R. Vukajlović, *Phys. Rev. Lett.* **76,** 960 (1996).
44. W. E. Pickett and D. J. Singh. *Phys. Rev. B* **53,** 1146 (1996).
45. T. Omata, K. Ueda, H. Hosono, M. Katada, N. Ueda, and H. Kawazoe, *Phys. Rev. B* **49,** 10194 (1994).
46. T. Omata, K. Ueda, H. Hosono, M. Miyazaki, S. Hasegawa, N. Ueda, and H. Kawazoe, *Phys. Rev. B* **49,** 10200 (1994).
47. M. A. Señarís-Rodríguez and J. B. Goodenough, *J. Solid State Chem.* **116,** 224 (1995).
48. M. A. Señarís-Rodríguez and J. B. Goodenough, *J. Solid State Chem.* **118,** 323 (1995).
49. R. Mahendiran, S. K. Tiwary, A. K. Raychaudhuri, R. Mahesh, and C. N. R. Rao, *Phys. Rev. B* **54,** R9604 (1996).
50. E. Iguchi, A. Tamenori, and N. Kubota, *Phys. Rev. B* **45,** 697 (1992).
51. H. Kawano, R. Kajimoto, M. Kubota, and H. Yoshizawa, *Phys. Rev. B* **53,** 2202 (1996).